Density functional theory based electron transport study of coherent tunneling through cyclic molecules containing Ru and Os as redox active centers

Xin Zhao and Robert Stadler*

Institute for Theoretical Physics, TU Wien, Wiedner Hauptstrasse 8-10, A-1040 Vienna, Austria

(Received 21 December 2018; revised manuscript received 1 February 2019; published 20 March 2019)

In our theoretical study in which we combine a nonequilibrium Green's function approach with density functional theory we investigate branched compounds containing Ru or Os metal complexes in two branches, which due to their identical or different metal centers are symmetric or asymmetric. In these compounds the metal atoms are connected to pyridyl anchor groups via acetylenic and phenyl spacer groups in a metaconnection. We find there is no destructive quantum interference (DQI) feature in the transmission function near the Fermi level for the investigated molecules regardless of their symmetry, either in their neutral states or in their charged states. We map the structural characteristics of the range of molecules onto a simplified tight-binding model in order to identify the main differences between the molecules in this study and previously investigated ferrocene compounds in order to clarify the structural sources for DQI, which we found for the latter but not for the former. We also find that local charging on one of the branches changes only the conductance by about one order of magnitude, which we explain in terms of the spatial distributions and charge-induced energy shifts of the relevant molecular orbitals for the branched compounds.

DOI: 10.1103/PhysRevB.99.115428

I. INTRODUCTION

Under the restrictions of low-bias current flowing through small molecules absorbed to metal electrodes in ultrahigh vacuum at very low temperature, the field of single-molecule electronics [1,2] has become accessible for a nonequilibrium Green's function (NEGF) approach combined with density functional theory (DFT) [3–7], which allows for an atomic interpretation of experimental results in a mechanical break junction or scanning tunneling microscope setup [8–11]. Destructive quantum interference (DQI) effects [12,13] allow for the design of logical gates [14] and memory cells [15] in single molecule electronics as well as the implementation of thermoelectric devices [16,17] since DQI is supposed to significantly reduce the conductance in conjugated π systems where such effects were even observed at room temperature [18].

Experimentally, the design and synthesis of branched compounds containing ferrocene moieties in each branch have been proposed [19] for the purpose of creating single-molecule junctions, where the combination of quantum interference effects with redox gating for coherent electron tunneling as well as the electrostatic correlation between spatially distinct redox centers for electron hopping [20] can be explored. A detailed theoretical analysis of branched compounds containing ferrocene centers was published in our previous work [21]. In order to assess the generality of this analysis we apply the same models and methods to cyclic $Me_2P(P(CH_3)_2)_8(C_2H_4)_4(C_6H_4)_4$ bis(pyridyldiacetylide) molecules (Fig. 1), where the two metal atoms Me are Ru or Os and we use the notation of Ru/Os, Os/Os, and Ru/Ru for complexes containing symmetrical and asymmetrical branches.

There are experimental and theoretical studies on coherent tunneling and electron hopping through single-branched molecules containing Ru atoms as redox active centers [20,22], where Ref. [20] focuses on the comparison between coherent tunneling and a hopping mechanism depending on the molecular length for ruthenium bis(pyridylacetylide) wires and the work in Ref. [22] investigated redox switches with coherent tunneling for the electron transport through the junction and the switching induced by hopping.

Cyclic analogs are of particular interest for the design of redox switches. If one of two redox centers is oxidized, the symmetry between the branches will be broken, thereby possibly enabling a DQI-induced suppression of the conductance. In that case the compound in Fig. 1 could be used as a molecular redox switch with very high on-off ratios. In our previous work on ferrocene-containing branched molecules we found that DQI occurs for neutral compounds in the energy region of the lowest unoccupied molecular orbital (LUMO) close to the Fermi level with a strong impact on the conductance only for molecules with branches connected in metapositions at the pyridyl anchors with respect to their N atom and containing acetylenic spacers regardless of the number of branches.

For the work on branched ferrocene compounds we used a simple but effective model, i.e., a combined atomic orbital (AO)/fragment orbital (FO) tight-binding (TB) model where we keep only the p_z AOs for each atom in both anchoring groups and one relevant bridge FO. For the molecules in Ref. [21] we found that the through-space coupling between the two anchor groups is the decisive parameter causing DQI effects even for single-branched molecules in the interesting energy region, i.e., in the gap between the highest occupied molecular orbital (HOMO) and the LUMO and close to the

*robert.stadler@tuwien.ac.at

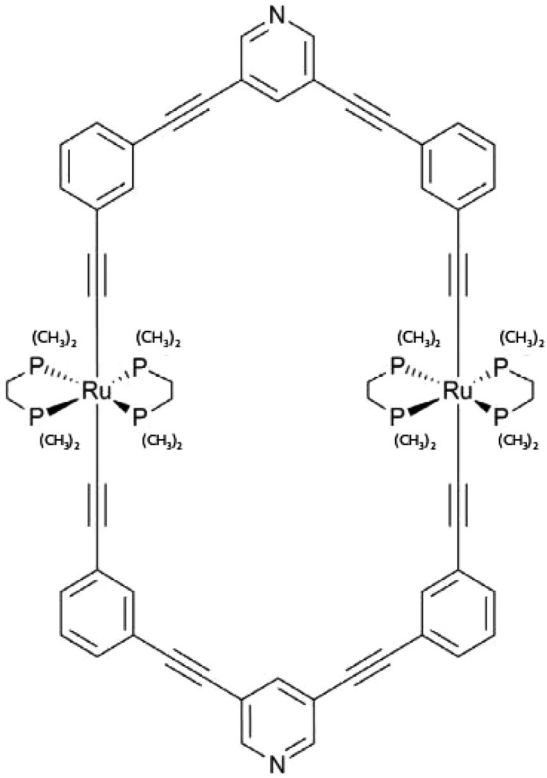

FIG. 1. Chemical structure of a cyclic $Ru_2(P(CH_3)_2)_8(C_2H_4)_4(C_6H_4)_4$ bis(pyridyl-diacetylide) molecule.

Fermi level E_F. For the molecules which are the focus of this study (Fig. 1) asymmetry can be introduced by exchanging one of the Ru redox centers with Os, and due to the longer organic bridges, the redox centers are more decoupled from the pyridyl anchors for these molecules than for the ferrocene compounds we studied in [21]. In this paper, we want to address two issues: (i) How do the TB models we used for the branched ferrocene molecules in Ref. [21] interpret coherent electron transport for this new type of molecule? (ii) Will the decreased through-space couplings due to the longer molecular length have an impact on the occurrence of DQI?

This paper is organized as follows: Sec. II gives the computational details for all NEGF-DFT calculations. In Sec. III we present transmission functions from these calculations for all junction geometries covered in this study and discuss their characteristics features, where comparisons of single- and double-branched molecules are made. In Sec. IV we derive tight-binding models which are topological in the sense that the transport Hamiltonian obtained from them contains explicitly only the bonding pattern of the described molecule, where atomic sites are represented by single AOs or fragments of the molecule by FOs. Detailed geometrical aspects such as distances and angles are only represented implicitly by the on-site energies and coupling strengths for these AOs and FOs, which we obtain from DFT calculations. The analysis scheme we employ was introduced in our previous study, where we found DQI for ferrocene-containing compounds and identified the structural sources for the absence of DQI in all Ru- and Os-containing compounds in the current study. In Sec. V we compare the conductance from NEGF-DFT calculations for charged systems with the corresponding neutral ones for assessing the usefulness of these double-branched systems as molecular switches. We conclude with a summary in Sec. VI.

II. COMPUTATIONAL DETAILS FOR THE NEGF-DFT CALCULATIONS

For the computation of transmission probabilities $\mathcal{T}(E)$, we performed DFT calculations with a Perdew-Burke-Ernzerhof (PBE) [23] exchange correlation (XC) functional within a NEGF framework [4–7] using a linear combination of atomic orbitals [24] as the basis set on a double-zeta level with polarization functions using the GPAW code [25,26], where a grid spacing of 0.2 Å for the sampling of the potential in the Hamiltonian on a real-space grid is used.

In our transport calculations, the scattering region is formed by the respective metal organic compounds and three and four layers for the upper and lower fcc gold electrodes, respectively, in a (111) orientation and with 6×10 gold atoms in the unit cell within the surface plane. The distance between the Au adatom attached to the electrodes surface and the N atom of the pyridyl anchor groups is 2.12 Å [27], and for the k points only the Γ point is used in the scattering region to evaluate $\mathcal{T}(E)$ due to the rather large cell sizes in our simulations.

The choice of electrode geometries with flat surfaces and a single Au adatom might be a bit arbitrary when compared with actual experiments, but in our experience from previous studies [28,29] a change in surface structure can lead to shifts of transmission functions on the energy axis due to altered Fermi level alignment but does not change the shape of the transmission function in terms of the occurrence or absence of DQI features in $T(E)$. The Fermi level of the electrodes would also always be situated within the energy range defined by the HOMO-LUMO gap regardless of the surface structure.

III. RESULTS AND DISCUSSION OF THE NEGF-DFT CALCULATIONS

In Fig. 2 we illustrate the molecular junctions derived from the compound in Fig. 1, where we vary the two metal atoms acting as redox centers to be Ru/Os, Os/Os, and Ru/Ru. In the resulting transmission functions $\mathcal{T}(E)$ for all three combinations and also for comparison of compounds with single-branched cases of Ru and Os, which we show in Fig. 3, the HOMO peaks are close to the Fermi level for all investigated systems. Hence, we expect the conductance to be dominated by the MOs below E_F.

Our definition of DQI is that the transmission through a system with more than one MO around E_F is lower than the sum of the individual contributions of these MOs to $\mathcal{T}(E)$ [29,30]. The exact energetic position of the Fermi energy within the HOMO-LUMO gap, which is also affected by the underestimation of this gap in our DFT calculations with a semilocal parametrization of the XC functional, will have a crucial impact on the quantitative value obtained for the conductance, but qualitatively, DQI will always result in a significant conductance lowering for the structures in which it occurs, regardless of the details of the Fermi level alignment [30].

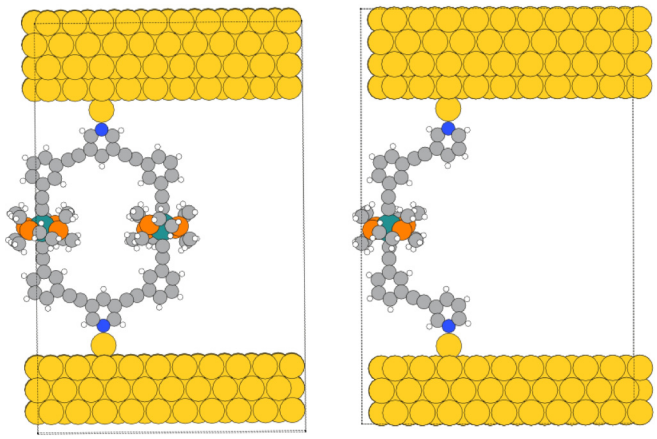

FIG. 2. Junction setups containing the molecule in Fig. 1, where for the double-branched molecule (left panel) the two metal atoms are varied as Ru/Ru, Ru/Os, and Os/Os and for the single-branched molecule (right panel) the single metal atom is either Ru or Os.

We note that for the molecule Ru/Os (green curve, Fig. 3) the peak splitting in the occupied region is distinct due to the intrinsic asymmetry caused by the different metal atoms in the two branches. In order to clarify whether there are DQI effects in the region of the HOMO-LUMO gap, we employ a simple TB model with a MO basis, where the eigenenergies of the molecular orbitals and their individual coupling values to the electrodes can be obtained by diagonalizing the subspace of the transport Hamiltonian with the basis functions centered on the molecule [21,31]. We use Larsson's formula [32–35],

$$\Gamma(E) = \sum_i \frac{\alpha_i \beta_i}{E - \varepsilon_i}, \tag{1}$$

with ε_i being the eigenenergy of each MO and α_i and β_i being its respective coupling to the left and right electrodes to calculate an approximation of the transmission function as

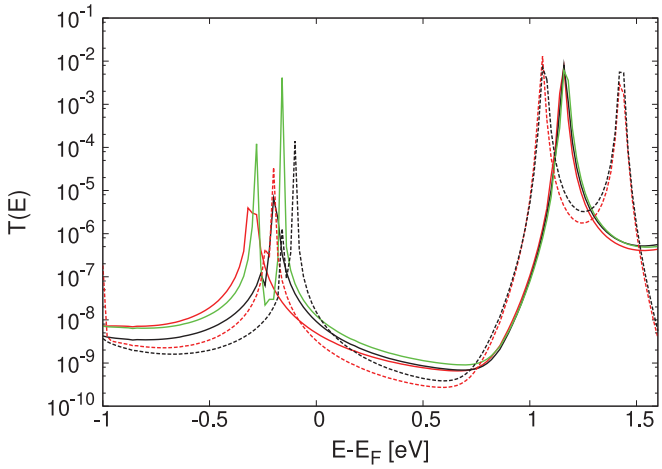

FIG. 3. Transmission functions from NEGF-DFT calculations for the double-branched molecules Ru/Ru (solid red line), Os/Os (solid black line), and Ru/Os (green solid line) as well as for single-branched Ru (dashed red line) and Os (dashed black line) in the junction setup shown in Fig. 2 in their neutral states.

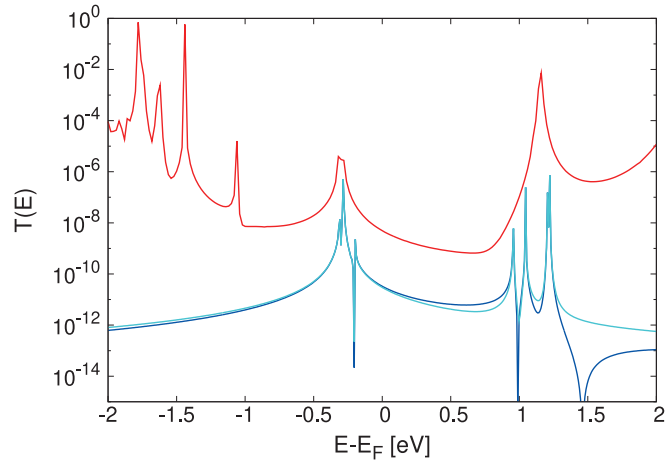

FIG. 4. Transmission functions calculated from NEGF-DFT (red curve) and Larsson's formula for the system Ru/Ru, where for the latter the blue curve denotes $(\mathrm{HOMO} + \mathrm{LUMO})^2$ and the cyan curve denotes $\mathrm{HOMO}^2 + \mathrm{LUMO}^2$.

$T(E) \sim \Gamma^2(E)$, where only the frontier orbitals, namely, the HOMO and the LUMO, are included, and we adopt the notation $\mathrm{HOMO} = (\alpha_{\mathrm{HOMO}}\beta_{\mathrm{HOMO}})/(E - \varepsilon_{\mathrm{HOMO}})$ and $\mathrm{LUMO} = (\alpha_{\mathrm{LUMO}}\beta_{\mathrm{LUMO}})/(E - \varepsilon_{\mathrm{LUMO}})$ in the following. As one can see from Fig. 4, the contributions from only the frontier molecular orbitals reproduce the characteristic features (blue curve) of the DFT result (red curve) for the molecule Ru/Ru. From Fig. 4 we also see that when the HOMO and LUMO are both coupled to the electrodes [$(\mathrm{HOMO} + \mathrm{LUMO})^2$, blue curve], we achieve a result identical to that from the individual contributions ($\mathrm{HOMO}^2 + \mathrm{LUMO}^2$, cyan curve) around E_F, which means no DQI of electron transport through these two MOs occurs for the system Ru/Ru. For all other systems, namely, Ru/Os, Os/Os, and single-branched Ru and Os, we obtain the same results (not shown here).

We also compare the transmission functions for single (red and black dashed lines) and double-branched (red and black solid lines) molecules to illustrate the impact of the number of branches in Fig. 3. As we can see, the transmission functions for the Ru (dashed red line) and Ru/Ru (solid red line) molecules are rather similar, and the zero-bias conductances differ only by a factor of about 1.5. The number of peaks in the occupied region for the double-branched molecule is higher than the one in the single-branched molecule as there are more molecular states coupled to the electrodes for the former. Comparing Os (dashed black line) and Os/Os (solid black line), we find the same qualitative differences, but the conductance for the double-branched molecule is now lower by about a factor of 0.6 for the single-branched molecule.

We already observed the deviation from the enhancement in the conductance of double-branched systems compared to the respective single-branched ones predicted theoretically [36,37] and demonstrated for some molecules experimentally in Ref. [38] in the ferrocene-containing compounds in our previous work [21], where we also discussed its origins in some length.

The next question is then what is the reason for the absence of DQI in the HOMO-LUMO gap when these molecules share

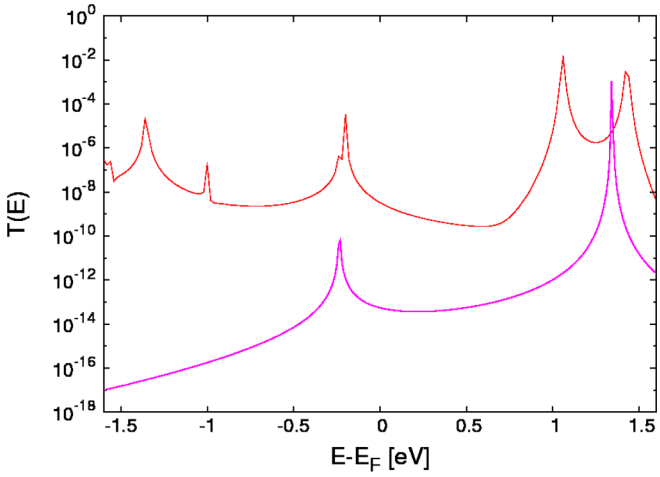

FIG. 5. Transmission functions for a single-branched Ru molecule, where the red curve is from a NEGF-DFT calculation. The magenta curve is obtained from a NEGF-TB calculation with one FO anchor state on each side and one bridge FO, where the anchor FO is obtained from a subdiagonalization of the transport Hamiltonian containing the p_z state of each carbon or nitrogen atom. For the electrodes a chain of single AOs with on-site energies of 0.83 eV and coupling values of −5.67 eV within the electrodes is used.

the design ideas with the ferrocene molecules we studied before [21]. In order to address this question we apply the AO-FO model we previously used for the ferrocene systems [21] in the next section and take the single-branched Ru molecule as an example due to its representative transmission function, which is very similar to those of the double-branched Ru/Ru, Os/Os, and Ru/Os and single-branched Os molecules.

IV. COMPARISON OF SIMPLIFIED 3 × 3 HAMILTONIANS FOR SINGLE- BRANCHED FERROCENE- AND RUTHENIUM-CONTAINING MOLECULES

Based on the scheme we developed in Ref. [21], we use the simplified 3 × 3 Hamiltonian in order to obtain a mathematical perspective for explaining the role of essential structural features for the occurrence or absence of DQI according to the following procedure, where we take single-branched Ru as an example. In the first step we define the p_z AOs of the anchor groups containing pyridyl and the attached acetylene moieties by diagonalizing the subspace of the transport Hamiltonian corresponding to each carbon or nitrogen atom on these groups and picking the p_z states, which can be identified by their on-site energies and symmetry. For the bridge group two relevant bridge FOs (again obtained by a subdiagonalization) in the occupied region are considered, where we define Ru plus phosphine ligands and conjugated spacers including the acetylene and benzene groups as part of the bridge. Then we diagonalize the two anchor group subspaces now defined only by p_z orbitals in order to get the relevant anchor FOs on both sides. We then minimize the Hamiltonian to the simplest one, which contains only the three most relevant states, i.e., one FO on each anchor group and one bridge FO. We show $\mathcal{T}(E)$ obtained from NEGF-TB calculations for such a three-FO model in Fig. 5 and find that if qualitatively reproduces the characteristic features found in NEGF-DFT calculations.

TABLE I. Parameters entering the 3 × 3 Hamiltonian formed by three FOs (Fig. 6) for three single-branched systems, where all values are given in eV. The values for Fc are obtained from the calculations presented in Ref. [21].

	Ru	Os	Fc
t_L	−0.026	−0.023	0.27
t_R	0.019	0.019	−0.22
t_D	5.7×10^{-5}	-5.1×10^{-5}	−0.023
$\Delta\varepsilon$	−1.5	−1.5	0.6

The most distinct differences between the molecules in Fig. 1 and those studied in Ref. [21] are the molecular length and the type of metal centers. In our previous work [21] we found that in order to observe a DQI feature close to E_F, the through-space coupling t_D needs to be neither too small nor too big in size so that the DQI feature will not be pushed outside the relevant energy region around E_F.

For a direct comparison of the molecules in our present study with those from our previous study we define the 3 × 3 Hamiltonian obtained from the three-FO model described above as

$$H_{\mathrm{mol}} = \begin{bmatrix} \varepsilon_L & t_L & t_D \\ t_L & \varepsilon_B & t_R \\ t_D & t_R & \varepsilon_R \end{bmatrix}$$

for the single-branched Ru, Os, and ferrocene (Fc) systems in Table I, where $\varepsilon_{L,B,R}$ are the respective on-site energies of the three FOs, $t_{L,R}$ are the electronic couplings between the two anchor FOs and the bridge FO, and t_D is the direct coupling between the anchor FOs.

We note that all junctions are rather symmetric, although not entirely when it comes to the relative orientation of the central molecule with regard to the Au slab on both sides within the surface plane. The opposite signs of t_L and t_R in Table I result from the symmetry of the bridge FO in Fig. 6(a) [it is the same as for Fig. 6(b) but more difficult to see there], where the FO localization pattern differs in sign at the connection points to the anchor FOs on the left and right sides.

We can see that the coupling values of t_L, t_R, and t_D connecting the three FOs for the three systems Ru, Os, and Fc differ in (i) the size of the couplings $t_{L/R}$ between the anchor and bridge, which is one order of magnitude smaller for Ru and Os compared with the ones in Fc, (ii) the through-spacing coupling t_D, which is three orders of magnitude smaller for the Ru and Os molecules, and (iii) the on-site energy ε_B of the bridge FO we used for the 3 × 3 Hamiltonian, which is the highest-lying FO in the occupied region for Ru and Os and was the lowest-lying FO in the unoccupied region for Fc. As a result the energy difference between anchor and bridge states $\Delta\varepsilon$ are larger in size for Ru and Os and the sign differs compared with the ferrocene molecule.

The differences in couplings can be interpreted by visualizing the FOs in Fig. 6, where the symmetry of the FOs on the anchors in Fig. 6(a) for the Ru molecule is equivalent to what is found for the ferrocene molecule [Fig. 6(b)], but $t_{L/R}$

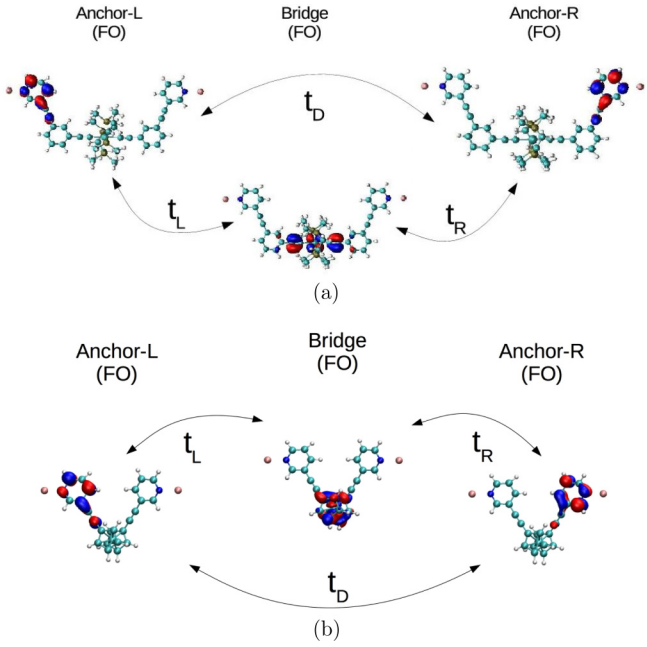

FIG. 6. Spatial distributions of the three FOs in the simplified model for (a) single-branched Ru with the anchor FO on each side at 1.3 eV and the bridge FO at −0.2 eV and (b) single-branched Fc with the anchor FO on each side at 1.05 eV and the bridge FO at 1.66 eV [21].

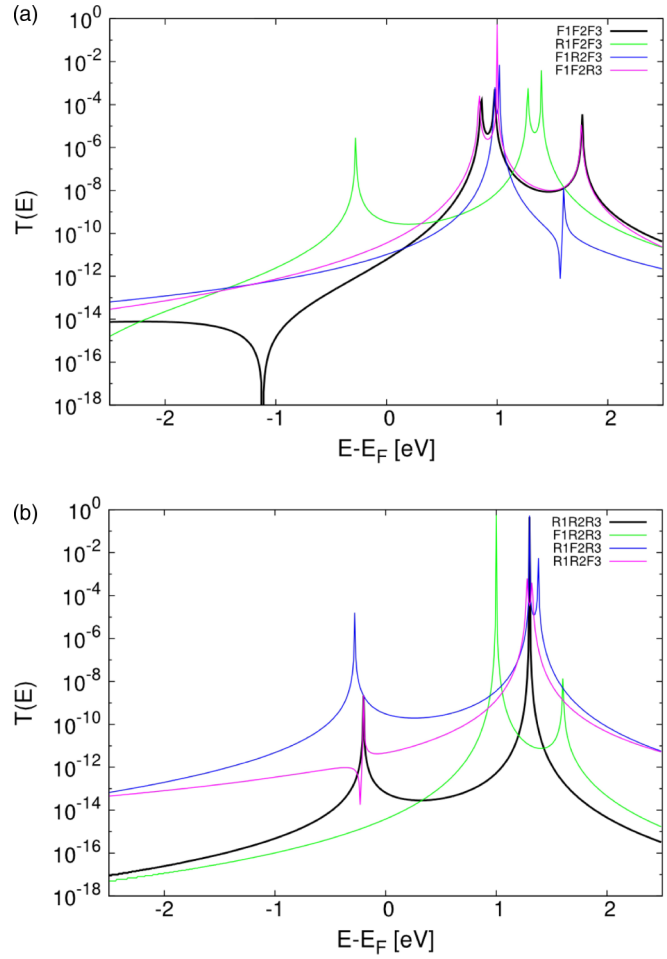

FIG. 7. Transmission functions obtained from NEGF-TB calculations using the 3FO model of the single-branched (a) Fc molecule (black solid line) and (b) Ru molecule (black solid line), where the symbols F and R represent Fc and Ru, respectively, and the indices 1–3 refer to the numbers in Table II. In (a) we start from the parametrization of Fc in Table II ($F_1F_2F_3$) and replace each of the parameters individually with the one corresponding to Ru and calculate $T(E)$ for $R_1F_2F_3$ (green line), $F_1R_2F_3$ (blue line), and $F_1F_2R_3$ (magenta line). In (b) we permute the parameters in the opposite direction, starting from the parametrisation of Ru in Table II ($R_1R_2R_3$) and obtaning $T(E)$ for $F_1R_2R_3$ (green line), $R_1F_2R_3$ (blue line), and $R_1R_2F_3$ (magenta line).

decreases markedly because in between the metal complex and the pyridyl group there is now a benzene unit separating the two for the Ru molecule. The benzene groups are defined as part of the bridge in our subdiagonalization, but the resulting bridge FOs close to E_F show no localization on them. In addition, the increased length also strongly reduces the direct coupling t_D between the two anchor groups. The bridge state on the Ru molecule is also localized on the adjacent triple bonds, while for Fc the state is confined to the ferrocene moiety.

Having established above that the parameters $t_{L/R}$, t_D, and $\Delta\varepsilon$ distinguish the ferrocene molecule with a DQI feature close to the LUMO from the single-branched systems Ru and Os, we want to further explore the relative importance of these parameters, where we focus on the comparison of Ru and Fc regarding the three parameters entering the Hamiltonian. If we mark the three parameters for the ferrocene molecule as F_1, F_2, and F_3 and those for Ru as R_1, R_2, R_3, where the numbers refer to those given in Table II, there are six possible combinations of them for forming a 3 × 3 Hamiltonian. From these Hamiltonians we calculate the transmission functions with NEGF-TB for each combination in order to identify the decisive parameters enabling DQI.

TABLE II. The three parameters defining the 3 × 3 Hamiltonian within the 3FO model which qualitatively reproduce the transmission function for the single-branched Ru and Fc systems.

	Ru	Fc
$\Delta\varepsilon$ (parameter 1)	−1.5	0.6
$t_{L/R}$ (parameter 2)	0.025	0.25
t_D (parameter 3)	5.0×10^{-5}	−0.023
$t_D/t_{L/R}$	-2.0×10^{-3}	−0.092

For the sake of simplicity we approximate the coupling values $t_{L/R}$ as 0.025 and 0.25 eV for Ru and Fc, respectively, and plot the transmission functions for the six resulting Hamiltonians based on different combinations of the three parameters in Fig. 7.

As one can see, modifying any one of the three parameters in the Hamiltonian of Fc leads to the disappearance of the DQI feature in the interesting region, which indicates that all three parameters have a fundamental influence on the absence of DQI for Ru in the relevant energy region and their interplay, which is decisive for the absence or occurrence of DQI features within the HOMO-LUMO gap. The through-space

coupling $t_D i$, however, is still special in the sense that taking the value from Fc in the Ru Hamiltonian [$R_1R_2F_3$ in Fig. 7(b)] induces a DQI minimum slightly below the HOMO peak.

In the following we keep two parameters fixed and vary one in a systematic way to further investigate the role each parameter plays. In Fig. 8 we illustrate the relation between each of these three parameters and the energy position of the DQI-induced minimum E_0, which we obtain from the eigenenergies and amplitudes at the contact sites of the three MOs resulting from a diagonalization of the parametrized 3×3 Hamiltonian corresponding to the three-FO model in combination with Larsson's formula [30] using the procedure described in detail in Ref. [21].

The so-obtained single-parameter dependencies can be summarized as linear for $E_0(\Delta\varepsilon)$ [Fig. 8(a)], as quadratic for $E_0(t_{L/R})$ [Fig. 8(b)], and as multiplicative inverse for $E_0(t_D)$ [Fig. 8(c)]. The black curve in Fig. 8(a) illustrates that for the single-branched Ru system with t_D and $t_{L/R}$ fixed to the values in Table II, E_0 lies always above $\sim$12 eV regardless of the variation of $\Delta\varepsilon$. For the Fc system (red curve in Fig. 8) E_0 is around -1.1 eV, i.e., close to E_F, for $\Delta\varepsilon$ chosen as in the real system but is pushed below -3 eV when the value is replaced by the one corresponding to the Ru molecule.

While E_0 shows a significant dependence on $t_{L/R}$ in Fig. 8(b) for both systems with a maximum at $t_{L/R} = 0$, they differ strongly in the sense that this maximum which is defined by ε_B corresponds to the LUMO peak for Fc and the HOMO peak for Ru, meaning that a variation of $t_{L/R}$ allows us to introduce a DQI minimum into the HOMO-LUMO gap only for the former and not for the latter. A variation of the parameter t_D on the other side allows for E_0 to cross the HOMO-LUMO gap for both systems, as can be seen from Fig. 8(c), albeit for values about an order of magnitude smaller for Ru when compared with Fc and for different signs.

We put our findings on the t_D dependence of E_0 to a test by performing NEGF-TB calculations for a range of values of t_D where $\Delta\varepsilon$ and $t_{L/R}$ have been kept fixed to the values for the Ru Hamiltonian in Table II. In Fig. 9(a) we show that the real value for Ru in Table II (0.00005 eV) is too small to cause DQI anywhere near the gap; a value larger by about one order of magnitude (0.0004 eV) makes a DQI feature appear above the LUMO, and if the value is too large (0.09 eV), the feature merges with the HOMO peak. An intermediate value (0.0002 eV) places the DQI-induced minimum optimally within the gap and close to the Fermi level, where its influence on the conductance will be most pronounced. In Fig. 9(b) we confirm the findings of Fig. 8(c), namely, that the sign of t_D matters significantly for the location of E_0.

For a physical interpretation of our results we note that the ratio $t_D/t_{L/R}$ we obtain from the optimal t_D value in Fig. 9(a) (0.002 eV), where we keep $t_{L/R}$ fixed to 0.025 eV, is 0.08, meaning that its magnitude is very close to that for the Fc system and about two orders of magnitude larger than the real value of t_D for the Ru molecule in Table II. It is intuitively plausible that this ratio plays such a significant role in the occurrence of DQI, where since it is a wave phenomenon, destructive interference needs two different pathways which are highly asymmetrical with respect to each other but not more than one order of magnitude apart in their respective couplings. In our model these two pathways are represented by the transport through the metal center via $t_{L/R}$ and the

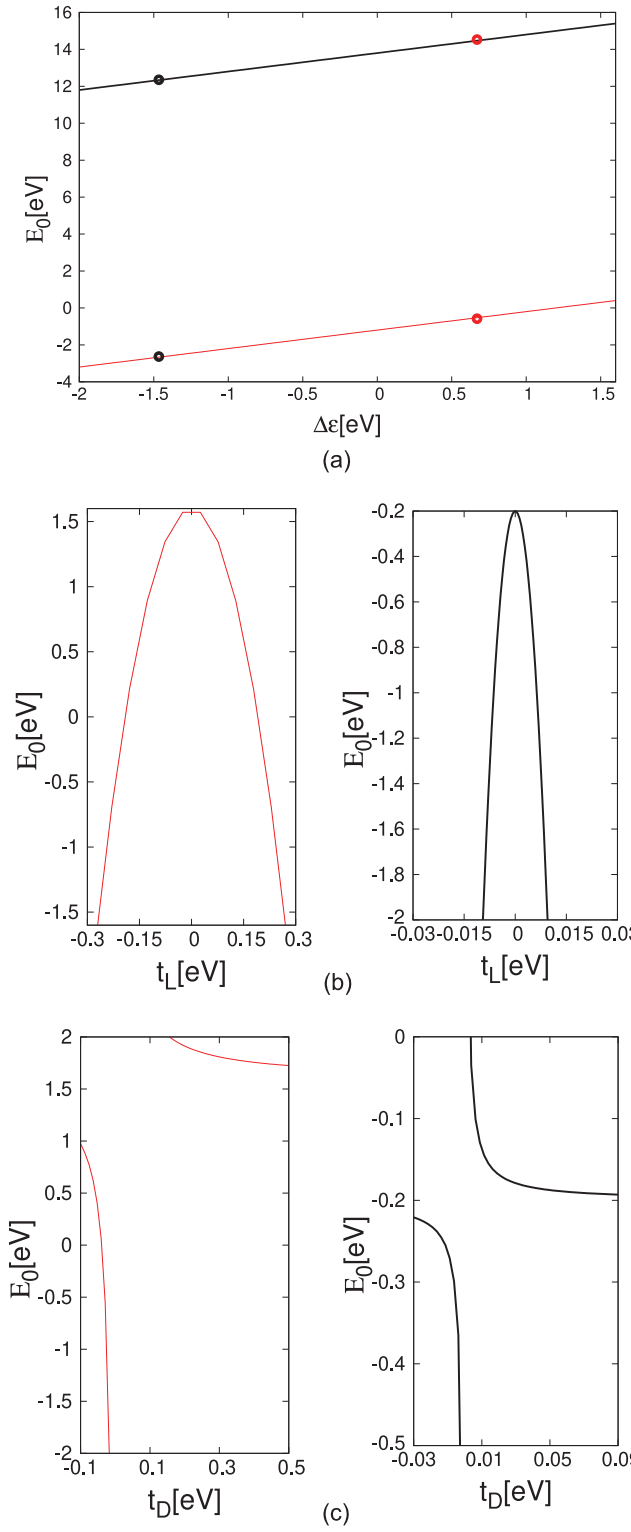

FIG. 8. E_0 versus (a) the energy difference $\Delta\varepsilon$ between the anchor and bridge states and (b) the coupling value $t_{L/R}$ and (c) t_D for Ru (black curve) and Fc (red curve). In (a) the E_0 values resulting from $\Delta\varepsilon$ (Ru) and $\Delta\varepsilon$ (Fc) at -1.5 and 0.6 eV are marked as black and red dots, respectively, while the values for $t_{L/R}$ and t_D are defined by the color of the line the dots are situated on.

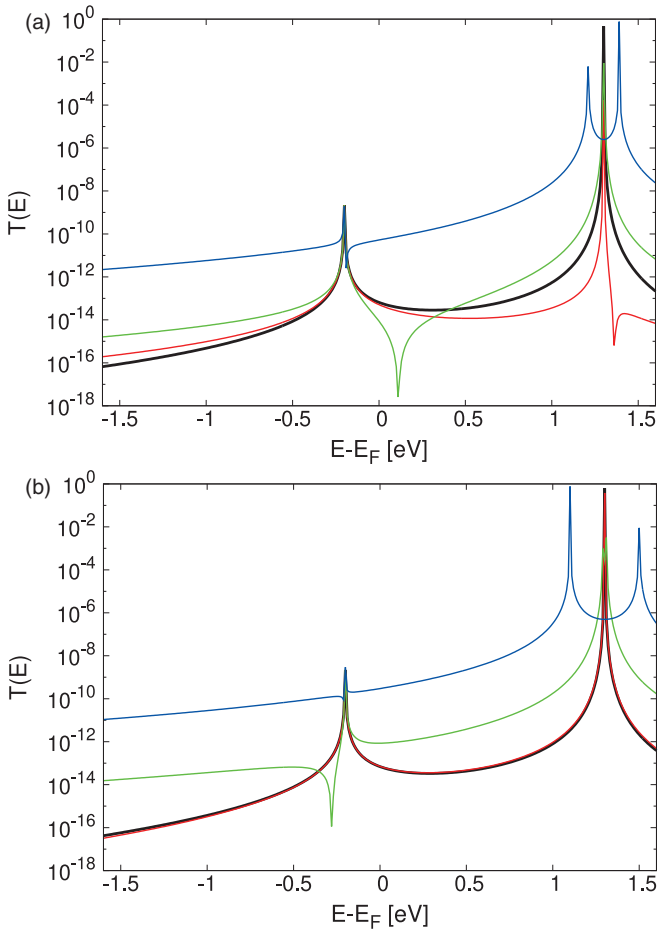

FIG. 9. Transmission functions calculated with NEGF-TB for the single-branched Ru system for (a) $t_D = 0.00005$ eV (black line), 0.0004 eV (red line), 0.002 eV (green line), and 0.09 eV (blue curve) and (b) $t_D = -0.00005$ eV (black line), -0.0001 eV (red line), -0.008 eV (green line), and -0.2 eV (blue line).

transport from anchor to anchor mediated by t_D, as also illustrated in Fig. 6. This seems to be a general rule regardless of the detailed quantitative values for $\Delta\varepsilon$, $t_{L/R}$, and t_D, which will facilitate the chemical design of molecules, enabling DQI in their electron transport characteristics in the future.

V. EFFECT OF CHARGING

In order to ensure the charge neutrality in the unit cell of the system, which is necessary also for a junction with a charged molecule when applying periodic boundary conditions for electronic-structure calculations, the countercharge to the complex has to be an explicit part of the cell, where we use Cl^- as a counterion (Fig. 10). We used the generalized Δ self-consistent field (SCF) method to calculate the charging effect in this section, where one additional electron on the chlorine p shell [31] is subtracted from the molecule. In this way the molecule is charged, and we keep the neutrality of the unit cell in our calculations. This approach makes use of the flexibility of the generalized Δ SCF method to define the spatial expansion of an orbital which is forced to contain an

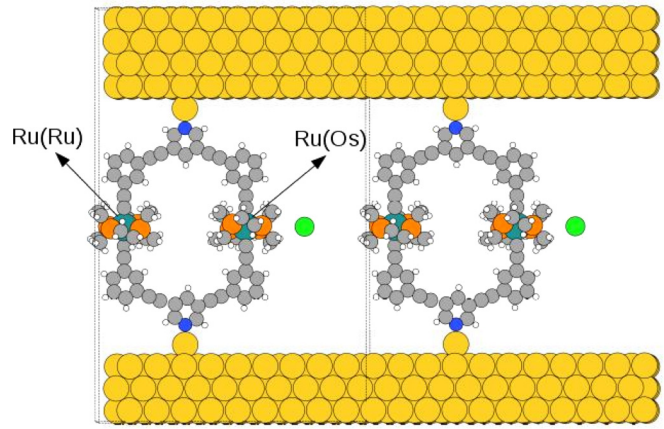

FIG. 10. Junction geometry for two neighboring cells in the periodic setup for the scattering region of double-branched Ru/Os containing a chlorine atom for achieving local charging with a distance of 5.2 Å between Cl and the closer-lying metal atom.

electron as an arbitrary linear combination of Bloch states [39,40] and in our calculations is localized on only a single Cl atom, as is predefined at the beginning of each iteration step. The self-consistency cycle then progresses as usual, but with the electron density of this particular orbital as a contribution to the external potential. In this way we can fix the electron occupation for the Cl manually, which solves the self-interaction problem implicitly and makes this method ideal for introducing localized charges into a junction [31].

The redox centers with localized d states on the metal atom in the investigated systems are stabilized by four donor ligands, which suggests a tetragonal ligand field [41]. According to ligand field theory, for an octahedral field with Jahn-Teller distortion, the orbitals $d_{x^2-y^2}$ and d_{z^2} are in higher-lying energy levels, and the orbitals d_{xz}, d_{yz} and d_{xy} are in lower-lying energy levels [22,42] [Fig. 11(a)]. We find that the peaks in the occupied region close to the Fermi level have contributions mostly from d orbitals with d_{xz} or d_{yz} symmetries [Fig. 11(b)], where d_{xy} lies farther below in energy [Fig. 11(c)]. For the systems investigated here the d orbitals d_{xz} and d_{yz} are fully occupied for all systems when in their neutral state, while for the charged state when Ru II is oxidized to Ru III [Fig. 11(a)], either d_{xz} or d_{yz} is singly occupied according to Hund's rule. This single occupation of a localized state leads to the necessity of spin polarization in our DFT calculations because spin-up and spin-down orbitals are then not equivalent in energy anymore.

From the respective MO eigenenergies within the junction in Fig. 11(c), which we obtained from a subdiagonalization of the transport Hamiltonian, it can be seen that for the asymmetric system, Ru/Os, the amount of the shift induced by charging is smaller than for the two symmetric systems, Ru/Ru and Os/Os. Ru/Os also differs from the other two molecules in the energetic sequence of the orbitals, where there are no degeneracies for this case and no changes in sequence when moving from the neutral to the charged system. We also show the difference for the energies of the MOs on the branch closer to Cl and on the other branch with respective

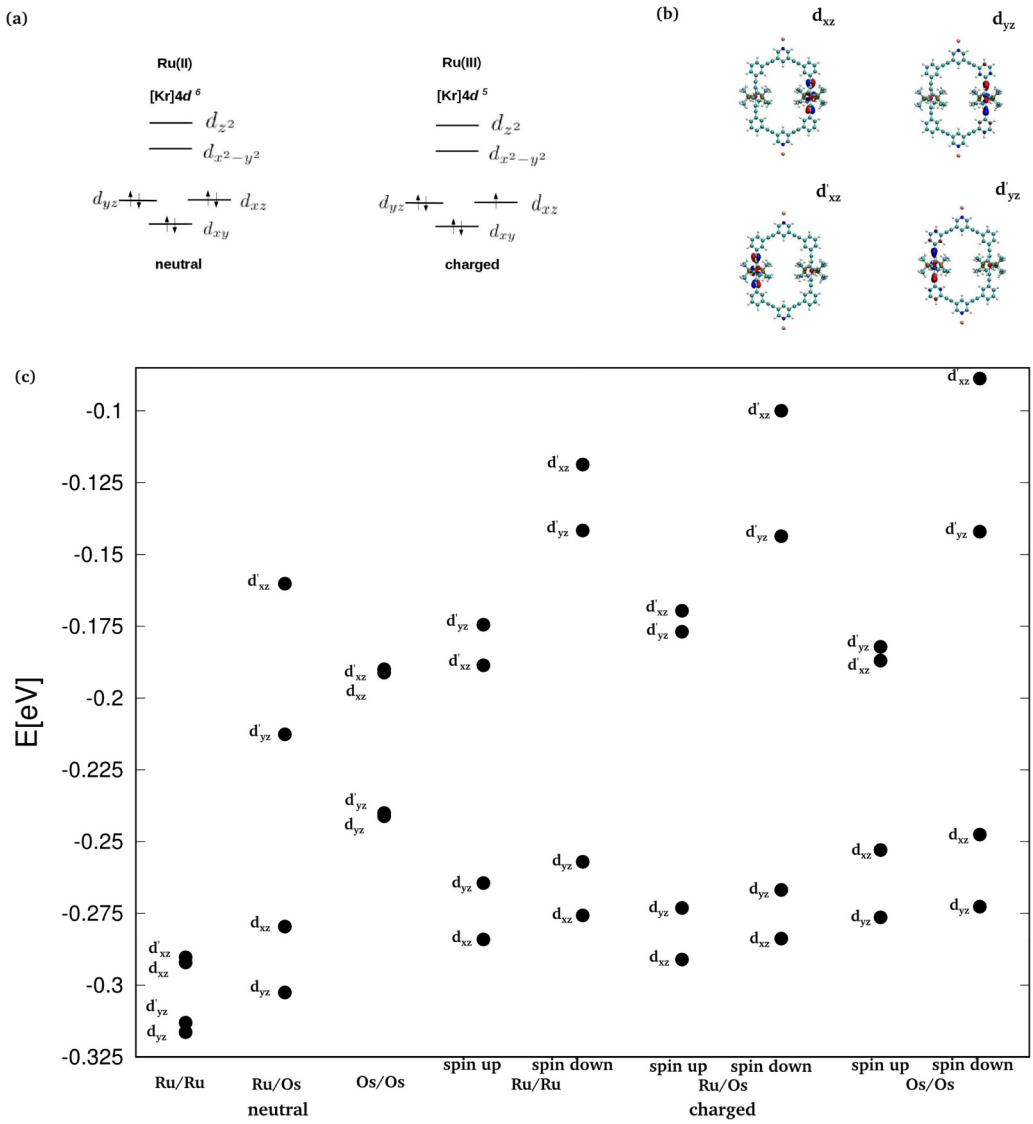

FIG. 11. (a) Electron occupation of the Ru d orbitals in a low-spin configuration for neutral and charged molecules according to ligand field theory, (b) spatial localization of the four relevant occupied orbitals, and (c) their corresponding energies within the junction and with respect to the Fermi level for three systems, namely, Ru/Ru, Ru/Os, and Os/Os in their neutral and charged states.

d_{xz} and d_{yz} symmetries in Table III, which confirms the same trends.

Since the PBE functional which we employ for the XC part in our NEGF-DFT calculations leads to an underestimation of the HOMO-LUMO gap where localized d states are particularly affected, the values for on-site energies shown in Fig. 11(c) and Table III cannot be directly compared with experiments. We, however, expect qualitative trends to be correctly reproduced as we assume the relative errors are the same for the three molecules we compare, as we did in a recent

TABLE III. Energy differences (in eV) between the occupied d orbitals close to E_F with symmetries d_{xz} and d_{yz} localized on the two branches M_1 and M_2, where M_2 is closer to the Cl atom and contains Os for the mixed case Ru/Os. For M_1 we mark the respective d orbitals as d_{xz} and d_{yz}, and for M_2 we mark them as d'_{xz} and d'_{yz}. We use the same notation as in Fig. 11 for all double-branched molecules in their respective neutral and charged states. For all systems we define $\Delta\varepsilon(d_{xz}) = d'_{xz} - d_{xz}$ and $\Delta\varepsilon(d_{yz}) = d'_{yz} - d_{yz}$.

	$\Delta\varepsilon(d_{xz})$			$\Delta\varepsilon(d_{yz})$		
	Ru/Os	Os/Os	Ru/Ru	Ru/Os	Os/Os	Ru/Ru
Neutral	0.120	0.001	0.002	0.090	0.001	0.003
Charged/spin up	0.121	0.064	0.098	0.096	0.094	0.090
Charged/spin down	0.184	0.159	0.157	0.123	0.131	0.115

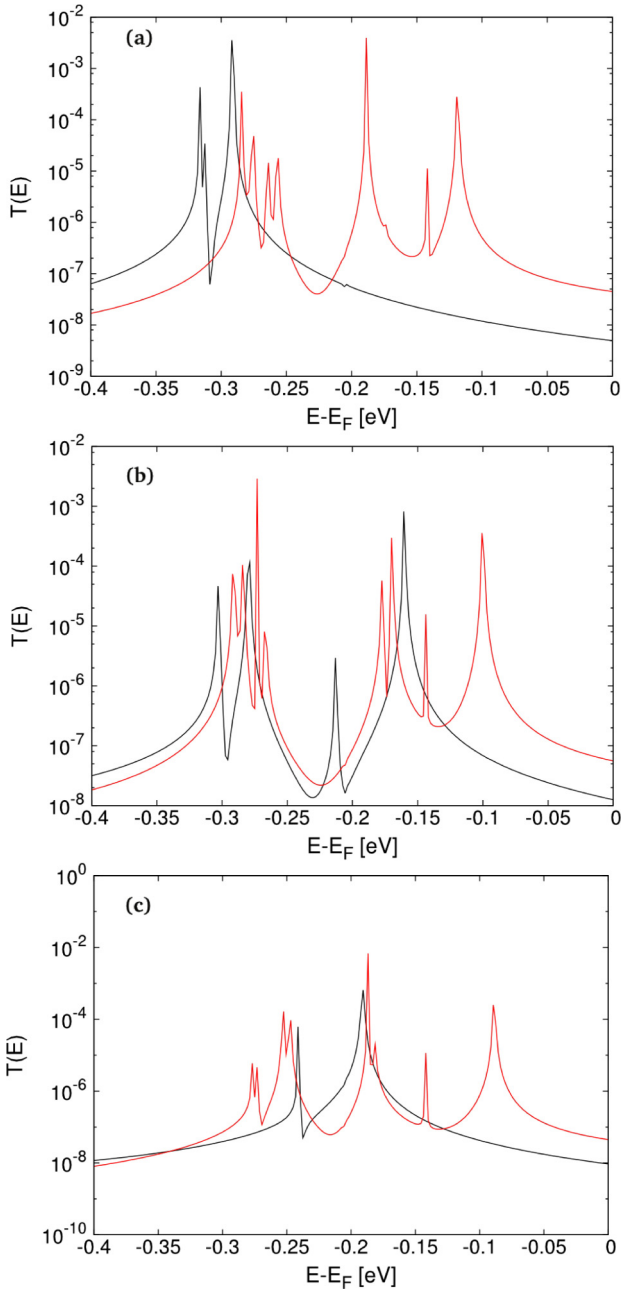

FIG. 12. Transmission functions for (a) Ru/Ru, (b) Ru/Os, and (c) Os/Os in their respective neutral (black solid line) and charged states (red solid line), where for the latter the average of spin-up and spin-down contributions has been used.

study on similar systems in which we also employed scissor operator corrections for a more quantitative comparison with experiments [43].

Figure 12 shows the transmission functions for each branched molecule in this study (Ru/Ru, Ru/Os, Os/Os) in their respective neutral and charged states, where we conducted spin-polarized NEGF-DFT calculations for all charged systems. It can be seen that the peak splitting for the two symmetrically built molecules, Ru/Ru and Os/Os, after charging is pronounced, where MOs on the branch closer to the chlorine atom shifted more with respect to the Fermi level and the MOs on the other branch have almost not been affected by the chlorine charging effect. For the asymmetrically built molecule, Ru/Os, the peak splitting caused by charging is less distinct because of the peak splitting already occurring in the neutral case due to the built-in asymmetry of the molecule, where charging does not seem to increase this splitting much further.

TABLE IV. Partial charges as obtained from a Bader analysis [44] for each of the two branches (metal complex plus all penyl and acetylene spacers but without the pyridyl anchors) of the double-branched neutral and charged molecules, where M_1 and M_2 denote the branch containing the metal center farther away from and closer to the chloride ion, respectively. All values for the charges are given in units of the norm of fractions of electrons, so that our notation is in agreement with the chemical picture where cations are marked with positive charges. The conductance G for all molecules as defined by $\mathcal{T}(E_F)$ is given in units of G_0.

	M_1	M_2	G
Ru/Ru (neutral)	0.038	0.037	4.94×10^{-9}
Ru/Ru (Cl)	0.208	0.662	4.48×10^{-8}
Ru/Os (neutral)	0.0345	0.0378	1.26×10^{-8}
Ru/Os (Cl)	0.173	0.710	5.58×10^{-8}
Os/Os (neutral)	0.036	0.036	9.19×10^{-9}
Os/Os (Cl)	0.230	0.653	4.46×10^{-8}

In Table IV we list the conductance of the neutral and charged states for each system as well as the partial charge on each molecule in order to investigate the sources of the asymmetry in MO energies as induced by charging and their effect on the coherent electron transport through the junction. While there is a marked difference between the partial charges on the two branches for the charged versions of all three molecules, the conductance of the charged systems changes only slightly when compared with their neutral counterparts since the energy shifts of the peaks in the occupied region are relatively small and the conductance is dominated by those rather narrow peaks. Therefore, we conclude that these molecules are not suitable for redox switches since although one of the two branches can be selectively oxidized, this does not result in a significant DQI-induced reduction of the conductance.

VI. SUMMARY

In this study we investigated the potential use of branched molecules containing different metal centers in two branches as molecular transistors where the switching would be achieved by a redox process, allowing us to alternate between an on and an off state, which would differ in their conductances by the occurrence of DQI effects in only one of these two redox states. We did not, however, find a DQI effect in the coherent electron transport through the branched molecules in our study, in either their neutral or charged states.

By comparing our results with previously studied ferrocene compounds, we further developed a scheme for the analysis of the structural conditions for the occurrence or absence of DQI in branched metal complexes with redox active groups in each branch. We found that the ratio of the through-space coupling

t_D and the couplings between anchor and bridge states $t_{L/R}$ play a decisive role in this context, which is significant for chemical design purposes. These parameters, however, are barely altered by the oxidation of one of the two branches. As a consequence, the charging effect on the conductance of these cyclic molecules is not pronounced, and only a rather moderate upward shift in energy of the narrow peaks in the transmission curves corresponding to occupied MOs on one branch is found.

Our findings and the analysis scheme we developed are likely to facilitate the design of DQI-based redox switches and to interpret experimental observations on such complex molecules in the future.

ACKNOWLEDGMENTS

X.Z. and R.S. both were supported by the Austrian Science Fund FWF (Project No. P27272). We are indebted to the Vienna Scientific Cluster VSC, whose computing facilities were used to perform all calculations presented in this paper (Project No. 70671). We gratefully acknowledge helpful discussions with G. Kastlunger.

[1] M. Ratner, Nat. Nanotechnol. **8**, 378 (2013).
[2] E. Lörtscher, Nat. Nanotechnol. **8**, 381 (2013).
[3] Y. Meir and N. S. Wingreen, Phys. Rev. Lett. **68**, 2512 (1992).
[4] M. Brandbyge, J. L. Mozos, P. Ordejon, J. Taylor, and K. Stokbro, Phys. Rev. B **65**, 165401 (2002).
[5] Y. Xue, S. Datta, and M. A. Ratner, Chem. Phys. **281**, 151 (2002).
[6] A. R. Rocha, V. M. Garcia-Suarez, S. W. Baily, C. J. Lambert, J. Ferrer, and S. Sanvito, Nat. Mater. **4**, 335 (2005).
[7] K. S. Thygesen and K. W. Jacobsen, Chem. Phys. **319**, 111 (2005).
[8] C. Joachim, J. K. Gimzewski, R. R. Schlittler, and C. Chavy, Phys. Rev. Lett. **74**, 2102 (1995).
[9] M. A. Reed, C. Zhou, C. J. Muller, T. P. Burgin, and J. M. Tour, Science **278**, 252 (1997).
[10] J. Reichert, R. Ochs, D. Beckman, H. B. Weber, M. Mayor, and H. V. Löhneysen, Phys. Rev. Lett. **88**, 176804 (2002).
[11] R. H. M. Smit, Y. Noat, C. Untiedt, N. D. Lang, M. C. van Hemert, and J. M. van Ruitenbeek, Nature (London) **419**, 906 (2002).
[12] M. Mayor, H. B. Weber, J. Reichert, M. Elbing, C. von Hänisch, D. Beckmann, and M. Fischer, Angew. Chem., Int. Ed. Engl. **42**, 5834 (2003).
[13] C. J. Lambert, Chem. Soc. Rev. **44**, 875 (2015).
[14] R. Stadler, S. Ami, M. Forshaw, and C. Joachim, Nanotechnology **15**, S115 (2004).
[15] R. Stadler, M. Forshaw, and C. Joachim, Nanotechnology **14**, 138 (2003).
[16] R. Stadler and T. Markussen, J. Chem. Phys. **135**, 154109 (2011).
[17] C. M. Finch, V. M. Garcia-Suarez, and C. J. Lambert, Phys. Rev. B **79**, 033405 (2009).
[18] C. M. Guedon, H. Valkenier, T. Markussen, K. S. Thygesen, J. C. Hummelen, and S. J. van der Molen, Nat. Nanotechnol. **7**, 305 (2012).
[19] M. S. Inkpen, T. Albrecht, and N. J. Long, Organometallics **32**, 6053 (2013).
[20] G. Kastlunger and R. Stadler, Phys. Rev. B **91**, 125410 (2015).
[21] X. Zhao, G. Kastlunger, and R. Stadler, Phys. Rev. B **96**, 085421 (2017).
[22] F. Schwarz, G. Kastlunger, F. Lissel, H. Riel, K. Venkatesan, H. Berke, R. Stadler, and E. Lörtscher, Nat. Nanotechnol. **11**, 170 (2016).
[23] J. P. Perdew, K. Burke, and M. Ernzerhof, Phys. Rev. Lett. **77**, 3865 (1996).
[24] A. H. Larsen, M. Vanin, J. J. Mortensen, K. S. Thygesen, and K. W. Jacobsen, Phys. Rev. B **80**, 195112 (2009).
[25] J. J. Mortensen, L. B. Hansen, and K. W. Jacobsen, Phys. Rev. B **71**, 035109 (2005).
[26] J. Enkovaara *et al.*, J. Phys.: Condens. Matter **22**, 253202 (2010).
[27] R. Stadler, K. S. Thygesen, and K. W. Jacobsen, Phys. Rev. B **72**, 241401(R) (2005).
[28] R. Stadler, J. Phys.: Conf. Ser. **61**, 1097 (2007).
[29] R. Stadler, Phys. Rev. B **80**, 125401 (2009).
[30] X. Zhao, V. Geskin, and R. Stadler, J. Chem. Phys. **146**, 092308 (2017).
[31] G. Kastlunger and R. Stadler, Phys. Rev. B **88**, 035418 (2013).
[32] S. Larsson, J. Am. Chem. Soc. **103**, 4034 (1981).
[33] M. A. Ratner, J. Phys. Chem. **94**, 4877 (1990).
[34] G. Kastlunger and R. Stadler, Phys. Rev. B **89**, 115412 (2014).
[35] P. Sautet and M.-L. Bocquet, Phys. Rev. B **53**, 4910 (1996).
[36] M. Magoga and C. Joachim, Phys. Rev. B **59**, 16011 (1999).
[37] C. Joachim, Nat. Nanotechnol. **7**, 620 (2012).
[38] H. Vazquez, R. Skouta, S. Schneebeli, M. Kamenetska, R. Breslow, L. Venkataraman, and M. S. Hybertsen, Nat. Nanotechnol. **7**, 663 (2012).
[39] J. Gavnholt, T. Olsen, M. Engelund, and J. Schiøtz, Phys. Rev. B **78**, 075441 (2008).
[40] T. Olsen, J. Gavnholt, and J. Schiøtz, Phys. Rev. B **79**, 035403 (2009).
[41] J. Bendix, T. Birk, and T. Weyhermüller, Dalton Trans., 2737 (2005).
[42] C. E. Schäffer, C. Anthon, and J. Bendix, Coord. Chem. Rev. **253**, 575 (2009).
[43] X. Zhao and R. Stadler, Phys. Rev. B **99**, 045431 (2019).
[44] R. S. Mulliken, J. Chem. Phys. **23**, 1833 (1955).